Received: 16 September 2021 | Revised: 20 December 2021 | Accepted: 29 December 2021

IET Nanobiotechnology

DOI: 10.1049/nbt2.12075

The Institution of Engineering and Technology WILEY

ORIGINAL RESEARCH

Hypnea musciformis-mediated Ag/AgCl-NPs inhibit pathogenic bacteria, HCT-116 and MCF-7 cells' growth in vitro and Ehrlich ascites carcinoma cells in vivo in mice

Rita Ghose | **A. K. M. Asaduzzaman** | **Imtiaj Hasan** | **Syed Rashel Kabir**

Department of Biochemistry and Molecular Biology, Faculty of Science, University of Rajshahi, Rajshahi, Bangladesh

Correspondence

Syed Rashel Kabir, Department of Biochemistry and Molecular Biology, Faculty of Science, University of Rajshahi, Rajshahi 6205, Bangladesh.
Email: rashelkabir@ru.ac.bd and rashelkabir@gmail.com

Funding information

Ministry of Science and Technology, Grant/Award Number: 39.009.002.01.00.057.2015–2016/922/Phys-362; Rajshahi University, Grant/Award Number: A-930/5/52/RU/Science-30/20-21

Abstract

In the present study, Ag/AgCl-NPs were biosynthesised using *Hypnea musciformis* seaweed extract; NPs synthesis was confirmed by a change of colour and observation of a razor-sharp peak at 424 nm by UV–visible spectroscopy. Synthesised nanoparticles were characterised by transmission electron microscopy, energy-dispersive X-ray spectroscopy, X-ray powder diffraction and Fourier transform infrared spectroscopy. Bacterial cell growth inhibition proves that the Ag/AgCl-NPs have strong antibacterial activity and cell morphological alteration was observed in treated bacterial cells using propidium iodide (PI). Ag/AgCl-NPs inhibited Ehrlich ascites carcinoma (EAC) cells, colorectal cancer (HCT-116) and breast cancer (MCF-7) cell line *in vitro* with the IC_{50} values of 40.45, 24.08 and 36.95 μg/ml, respectively. Initiation of apoptosis in HCT-116 and MCF-7 cells was confirmed using PI, FITC-annexin V and Hoechst 33342 dye. No reaction oxygen species generation was observed in both treated and untreated cell lines. A significant increase of ATG-5 gene expression indicates the possibility of autophagy cell death besides apoptosis in MCF-7 cells. The initiation of apoptosis in EAC cells was confirmed by observing caspase-3 protein expression. Ag/AgCl-NPs inhibited 22.83% and 51% of the EAC cell growth *in vivo* in mice when administered 1.5 and 3.0 mg/kg/day (i.p.), respectively, for 5 consequent days.

KEYWORDS

Ag/AgCl-NPs, cell growth inhibition, gene expression, *Hypnea musciformis*, morphological study

1 | INTRODUCTION

In recent periods, cancer is a serious disease, and globally, it is the second leading cause of death. According to a WHO report in 2018, globally, 9.6 million deaths occurred due to cancer. Cancer deaths are increasing in low- and middle-income countries [1] and Bangladesh is a country where the number of cancer patients is gradually rising. According to cancer statistics in Bangladesh, about 0.2 million cancer patients are diagnosed each year [2]. Many synthetic drugs are available in the market for cancer eradication but are not satisfactory to patients. Serious side effects occur that lead to death of patients. Depending on patient demand, scientists are searching for a new drug for cancer eradication with reduced side effects.

As alternative anticancer and antimicrobial agents, metal nanoparticles are gradually gaining more importance in the biomedical area. Green synthesis of plant extract-mediated silver nanoparticles (AgNPs) has attracted researchers for the use of natural resources and their eco-friendliness, benignancy and rapid production, and they do not produce toxic by-products. Various bioactive molecules are present in plants that participate in the formation of AgNPs.

Plant-mediated AgNPs have become increasingly popular as antibiotic agents in textiles and wound dressings, medical devices and appliances such as refrigerators and washing machines. Many researchers already reported the antibacterial activity of plant-mediated AgNPs [3–5]. Nowadays, AgNPs have gained increased attention due to their promising role as

anticancer agents [6, 7]. Several scientists reported that AgNPs inhibited the L929 cells, DLA cells, Hep2 cells, MCF-7 cells, HT29 cells and Ehrlich ascites carcinoma (EAC) cell growth in a dose-dependent manner [8–11]. Recently, more than 60% of anticancer drugs are being invented from plants, microbes and marine organisms' natural resources [12, 13]. Natural resource-derived drugs have fewer side effects and act more specifically than synthetic drugs [14].

Hypnea musciformis is red in colour, sometimes yellowish-brown colour. The nutritive value of red seaweed is very high. It contains a lot of protein, vitamins, minerals, electrolytes, natural antioxidants, fibres and little amount of fat [15]. Marine sources have an important aspect as antibacterial and anticancer agents due to the presence of bioactive molecules. Different seaweeds have been reported as sources for the synthesis of AgNPs with antibacterial and anticancer properties [16, 17]. We have found three published articles on *H. musciformis*-synthesised AgNPs. One involves only synthesis [18], the second one involves nanoparticle synthesis and activity against *Aedes aegypti* and *Plutella xylostella* [19] and the third one involves nanoparticle synthesis and activity against *Xanthomonas campestris* and *Ralstonia solanacearum* [20]. But till now, *H. musciformis*-mediated Ag/AgCl-NPs with oral antibacterial and anticancer properties have not been reported in the literature. Therefore, our research work's total point was to study the antibacterial and antitumour properties of *H. musciformis*-mediated Ag/AgCl-NPs. Green synthesised Ag/AgCl-NPs was formed by *H. musciformis* extract and it was characterised by UV-vis spectroscopy, transmission electron microscopy (TEM), energy-dispersive X-ray spectroscopy (EDX), X-ray powder diffraction (XRD) spectra and Fourier transform infrared spectroscopy (FTIR). Additionally, the efficacy of Ag/AgCl-NPs inhibition against two pathogenic bacteria was evaluated and cell morphological alteration was monitored by propidium iodide (PI). Furthermore, anticancer properties of Ag/AgCl-NPs were checked in EAC cells in vivo and colorectal cancer (HCT-116), and breast cancer (MCF-7) cell line in vitro. Ag/AgCl-NPs-induced apoptotic cell death in EAC, HCT-116 and MCF-7 cells was detected by caspase-3 protein expression, PI, FITC-annexin V and Hoechst 33342 dye. Besides apoptosis, autophagy cell death in MCF-7 cells was also evaluated by gene expressions.

2 | MATERIALS AND METHODS

2.1 | Sample preparation

Sample was prepared according to the modified method by Venkatesan et al. [21]. Firstly, seaweed (*H. musciformis*) was collected from the Cox's Bazar region of Bangladesh and was washed with tap water and dried in sunlight. Then, it was powdered by a blender machine and homogenised with distilled water at a 1:100 ratio (w/v) for 15 min at 90°C. The homogenate was filtered two times by a muslin cloth. Subsequently, it was centrifuged to get a clear solution at 6000 g for 15 min. Finally, a clear light brown-coloured supernatant solution or extract was collected in a falcon tube and kept at 4°C.

2.2 | Ag/AgCl-NPs synthesis

Freshly prepared silver nitrate solution (1.0, 2.0 and 3.0 mM) was mixed with *H. musciformis* extract at a 1:1 ratio (v/v). The mixture solution was kept in sunlight at different reaction times (1, 2 and 4 h) for Ag/AgCl-NPs synthesis.

2.3 | Characterisation of the synthesised nanoparticles

The formation of nanoparticles was confirmed by UV–visible spectra analysis; morphological characterisation was carried out by TEM analysis; elemental characterisation was completed by EDX analysis; structural characterisation was carried out by XRD analysis and functional characterisation was carried out by FTIR analysis according to Kabir et al. [22] and the method is provided in supporting information S1.

2.4 | Growth inhibition assay of HCT-116, MCF-7 and EAC cells *in vitro*

In vitro, EAC cell growth inhibition was performed following the method by Kabir et al. [22, 23] with a slight modification and provided in supporting information S1.

2.5 | Propidium iodide and FITC-Annexin V staining

Ag/AgCl-NPs treated and untreated cells were performed using a FITC-annexin V and PI detection kit (ebioscience). First, HCT-116 and MCF-7 cells (2 × 104/well) were seeded in a 96-well culture plate, and after 24 h, three wells of cells were treated with 20 μg/ml concentration of *H. musciformis* extract-mediated Ag/AgCl-NPs, respectively, for 48 h. Untreated wells with cells were used as control. According to the manufacturer's (US Ever Bright) direction, cells were stained with PI and annexin V. Finally, cell morphological changes were observed by using a fluorescence microscope (Olympus IX71).

2.6 | Study of cell nuclei change by Hoechst 33342 staining

Around 10,000 HCT-116 and MCF-7 cells were seeded in each well of a 96-well cell culture plate and then treated with 20 μg/ml concentration of Ag/AgCl-NPs for 48 h as described above. After that, the cells were rinsed with phosphate buffer saline and stained with Hoechst 33342, according to Kabir et al. [22]. Finally, cell morphology was observed under both dark and bright fields using a fluorescence microscope.

2.7 | Observation of changes of the reactive oxygen species

After treatment with 20 μg/ml of Ag/AgCl-NPs, changes of the reaction oxygen species (ROS) level in the HCT-116 and MCF-7 cells were detected using 2′,7′-dichlorofluorescein-diacetate (DCFH-DA) staining. Cells were cultured in a 96-well plate and treated with Ag/AgCl-NPs for 48 h as described above. Cells were washed once by the serum-free medium and incubated with diluted DCFH-DA (1:1000) at 37°C for 20 min, and finally, the cells were examined by a fluorescence microscope.

2.8 | mRNA expression by real-time polymer chain reaction

For RNA isolation, MCF-7 cells (16 × 104/well) were seeded in a 6-well cell culture plate. After that, it was treated with 64 μg/ml concentration of Ag/AgCl-NPs. Untreated cells were used as control. After the 48-h incubation period, the next procedure was followed according to the method by Kabir et al. [24]. Forward and reverse primers were used for the reaction stated in Table S1.

2.9 | EAC cells growth inhibition assay *in vivo* in mice

EAC cell growth inhibition was determined according to Kabir et al. [25] and provided in supporting information S1.

2.10 | Caspase-3 protein expression assay

After cell separation from mice, the treated (3.0 mg/kg/day) and untreated EAC cells were incubated with the US Ever Bright super view-488 caspase-3 substrate for 30 min according to the manufacturer's guideline. Finally, cell morphology was examined using a fluorescence microscope described by Kabir et al. [26].

2.11 | Bacterial cell growth inhibition by MTT colourimetric assay

Bacterial cell growth inhibition was performed by 3-(4,5-dimethylthiazol-2-yl)-2,5-diphenyltetrazolium bromide (MTT) assay according to Kabir et al. [22] and provided in supporting information S1.

2.12 | Zone of bacterial growth inhibition by disc diffusion assay

Antibacterial activity of the synthesised Ag/AgCl-NPs was determined using the agar well diffusion assay method and furnished in supporting information S1.

2.13 | Antibiofilm assay

Antibiofilm assay was performed to observe film formation on top of the bacterial nutrient broth in test tubes with and without Ag/AgCl-NPs according to the method by Hasan et al. [27] and provided in supporting information S1.

2.14 | Bacterial cell morphological study by propidium iodide

Bacterial cells were treated with 32 μg/ml of Ag/AgCl-NPs to observe the morphological change. Details are given in supporting information S1.

3 | RESULTS

3.1 | Ag/AgCl-NPs formation

For Ag/AgCl-NPs formation, we added 1.0 ~ 3.0 mM of the silver nitrate solution in *H. musciformis* extract at a 1:1 ratio (v/v). After that, it was kept in sunlight for reaction at different times. The intensity of the solution colour increased from light red to deep brown with increased $AgNO_3$ concentrations for each reaction time, which is shown in Figure 1a–c. UV-Visible spectra were measured from 285 to 700 nm to confirm the formation of Ag/AgCl-NPs. A sharp peak around 424 nm was observed in the test tube containing 2 mM $AgNO_3$ at 2 h incubation as shown in Figure 1c–e. At that condition, nanoparticles were synthesised for further studies.

3.2 | Characterisation of the synthesised nanoparticles

The spherical shape observed in synthesised Ag/AgCl-NPs using TEM that was well monodispersed is shown in Figure 2a. The average particle size was estimated as 11 nm calculated by image J software shown in Figure 2b. The 3 KeV is a typical silver peak region. Metallic silver nanocrystalline absorption occurs at this region due to surface plasmon resonance. The presence of elemental Ag, C and Cl in the synthesised Ag/AgCl-NPs was confirmed by EDX as shown in Figure 2c. Different XRD reflection peaks 27.72°, 32.14°, 46.24°, 54.76°, 57.32° and 67.26° indicate the following crystallographic planes (111), (200), (220), (311), (222) and (400), respectively. The above-mentioned peak points out the formation of AgCl-NPs compared to card no. 00-901-1666. In contrast, we also identified other XRD reflection peaks 38.10° and 44.32° that indicate the crystallographic planes (111) and (200), respectively. Compare to card no. 00-150-9146, the above two peaks identified the formation of AgNPs (Figure 2d). *H. musciformis* extract shows different major peaks at 3427.88, 1639.74, 1384.42, 1097.33 and 618.04 cm^{-1}. On the contrary, the FTIR spectrum of synthesised Ag/AgCl-NPs shows the major peaks at 3411.45, 2920.32, 1631.03, 1384.13, 1101.1 and 618.34 cm^{-1} (Figure 2e,f).

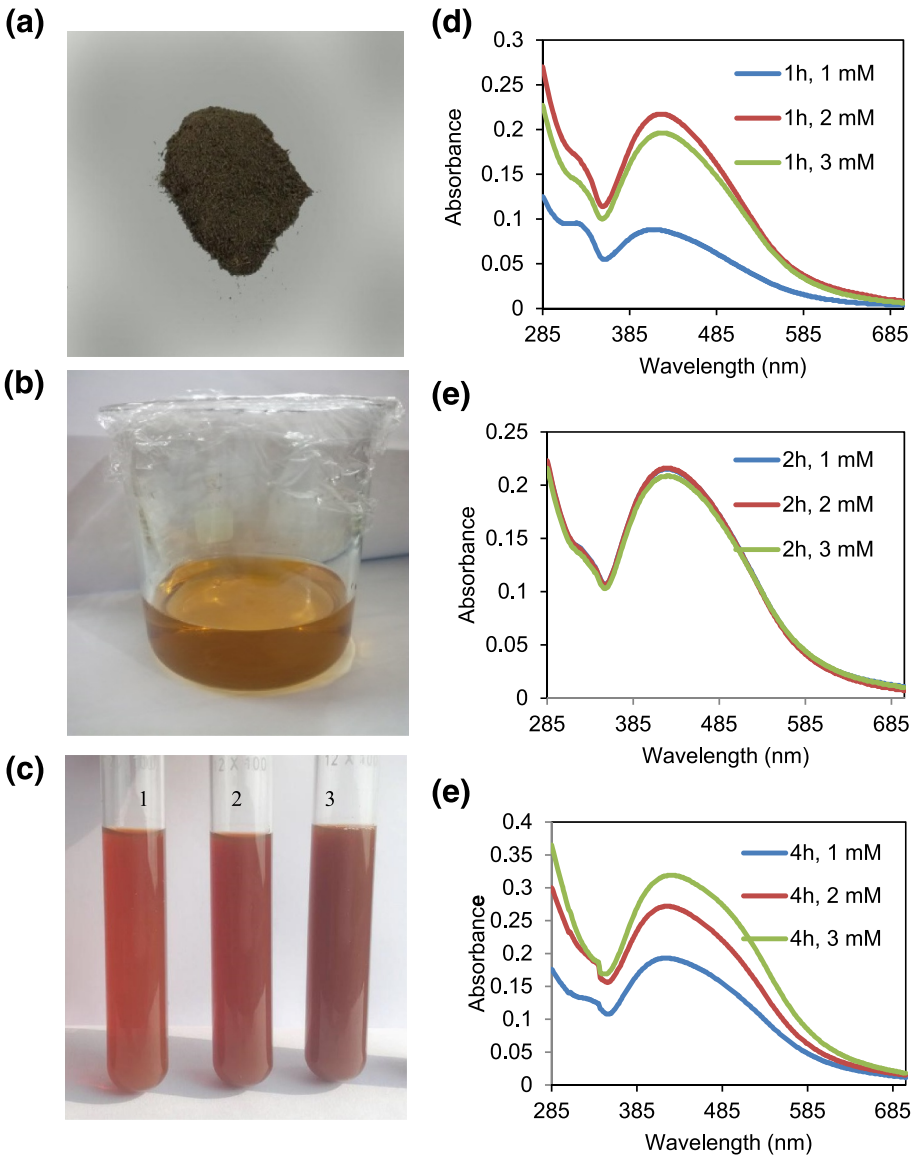

FIGURE 1 The formation of Ag/AgCl-NPs was identified by a colour change and UV–visible spectra: (a) *Hypnea musciformis* powder; (b) *H. musciformis* extract; (c) after reaction between silver nitrate and *H. musciformis* extract. (1) 1 mM $AgNO_3$; (2) 2 mM $AgNO_3$; (3) 3 mM $AgNO_3$. UV–visible spectra of the reaction mixture at different concentrations of $AgNO_3$ and reaction time during the synthesis of *H. musciformis* extract-mediated Ag/AgCl-NPs; (d) 1–3 mM $AgNO_3$, 1 h; (e) 1–3 mM $AgNO_3$, 2 h; (f) 1–3 mM $AgNO_3$, 4 h

3.3 | Antibacterial activity

MTT assay was used to investigate the effect of Ag/AgCl-NPs on oral bacterial cell growth inhibition. The Ag/AgCl-NP-induced bacterial cell growth inhibition was found to dose reliant focussed in Figure 3a,b. At 32 μg/ml, the inhibitory effect was 89.20% and 82.71% for *Staphylococcus aureus* and *Streptococcus mutans*, respectively, and it progressively declined to 57.46% and 51.66% at 4 μg/ml. Additionally, the significant zone of bacterial growth inhibition was observed against both bacteria shown in Table 1.

3.4 | Identification of apoptosis by propidium iodide

After using PI staining in Ag/AgCl-NP-treated *S. aureus* and *S. mutans* bacterial cells, a considerable number of red colour containing apoptotic bacterial cells were observed by a fluorescence microscope (Figure 3c).

3.5 | Antibiofilm activity

H. musciformis extract-mediated Ag/AgCl-NPs inhibited biofilm formation against *S. mutans* and *S. aureus* at different concentrations shown in Table S2. There was no visualised biofilm formation up to 96 h in *S. mutans* and *S. aureus* by using 20 μg/ml of Ag/AgCl-NPs.

3.6 | Cell growth inhibition *in vitro* and *in vivo*

Ag/AgCl-NPs inhibited the EAC, HCT-116 and MCF-7 cells growth inhibition in a dose-dependent manner (Figure 4a,b). The IC_{50} values were calculated to be 40.45 μg/ml, 24.08 and 36.95 μg/ml, respectively. Besides the EAC cell growth inhibition *in vitro*, Ag/AgCl-NPs had effectively inhibited EAC cell growth inhibition in vivo in mice. We found 22.83% of EAC cells growth inhibition at the dose of 1.5 mg/kg/day. But when the dose was

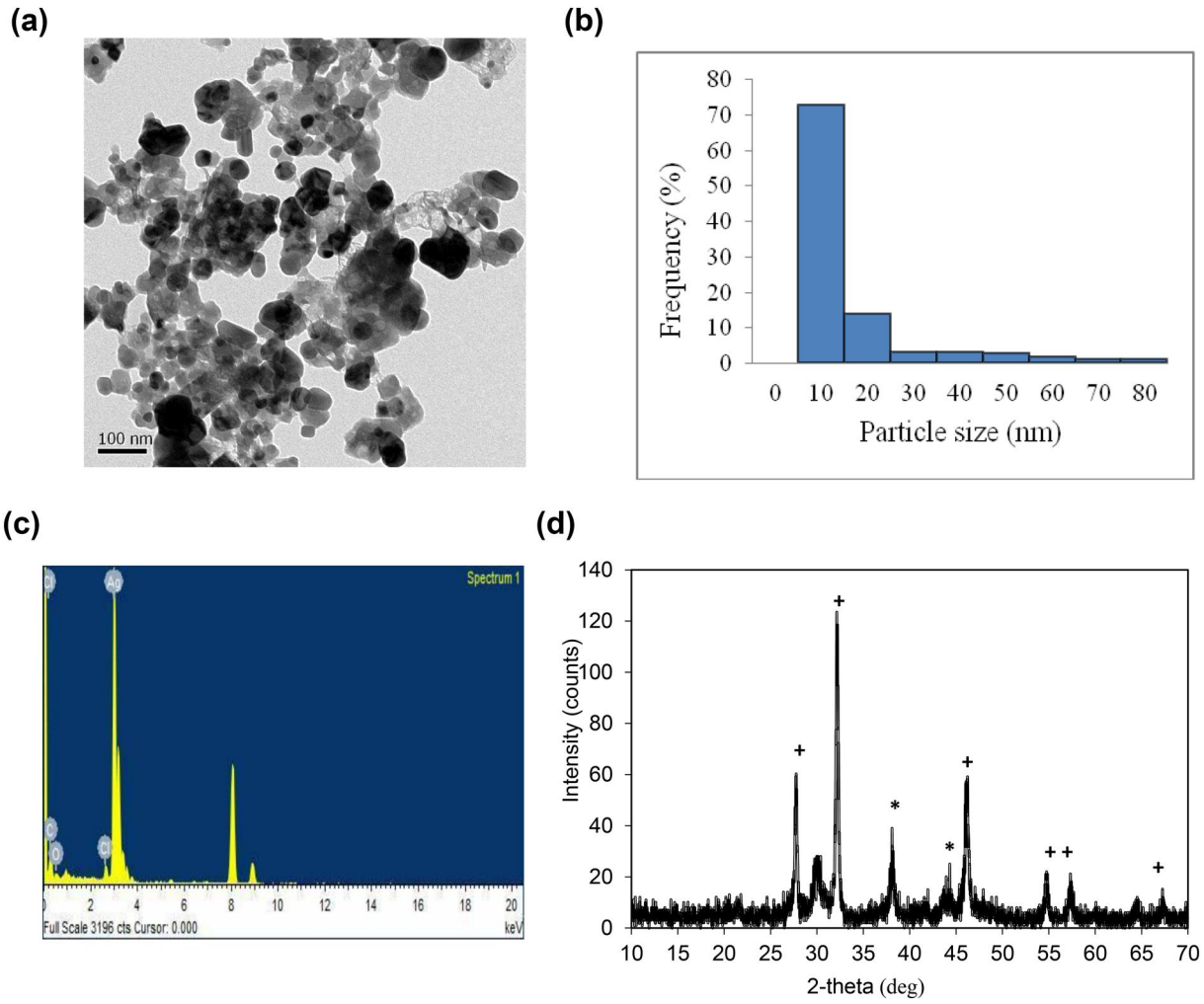

FIGURE 2 Characterisation of *Hypnea musciformis* extract-mediated Ag/AgCl-NPs. (a) Transmission electron microscopy micrograph showing the formation of Ag/AgCl-NPs. Inset: black solid bar indicating 100 nm. (b) Frequency distribution of synthesised Ag/Agcl-NPs. (c) The energy dispersive X-ray spectrum of Ag/AgCl-NPs. (d) X-ray powder diffraction (XRD) pattern of synthesised Ag/Agcl-NPs (+) and (*) indicating AgCl-NPs and silver nanoparticles (AgNPs), respectively. (e) Fourier transform infrared (FTIR) spectrum of *H. musciformis* extract. (f) FTIR spectrum of synthesised Ag/AgCl-NPs

increased to 3.0 mg/kg/day, the cell growth inhibition rose to 51% (Figure 4c).

3.7 | Induction of apoptosis by different fluorometric assays

After treatment with the Ag/AgCl-NPs, morphological changes in cells, early and late apoptotic features and no ROS production in the microscopic image of HCT-116 and MCF-7 cells were detected as presented in Figure 5a,b, respectively.

3.8 | Detection of caspase-3 protein and gene expressions

We used an optical and fluorescence microscope to observe the morphological examination of Ag/AgCl-NPs treated and untreated EAC cells. A round shape was observed in untreated cells, whereas a morphological variation was observed in treated cells using an optical microscope focussed in Figure 6a. By using a fluorescence microscope, the green colour cell image was not visualised in the untreated EAC cell surface. However, the image of the cells was green in treated EAC cells (Figure 6a). It might have happened due to substrate bound with caspase-3 that indicates the induction of apoptosis. We treated *H. musciformis*-mediated Ag/AgCl-NPs on MCF-7 cells to determine the expression level of apoptosis-related genes by real-time polymer chain reaction. In this study, ATG-5 gene expression level was increased by several times, whereas FAS, BAX and Bcl-2 gene expression level was decreased. A little rise in NFκB gene expression was also found (Figure 6b).

4 | DISCUSSION

Seaweeds have many bioactive compounds [28, 29] and possibly they are used as reducing and capping agents to synthesise biogenic nanoparticles. In the present study, we have green synthesised Ag/AgCl-NPs from the *H.*

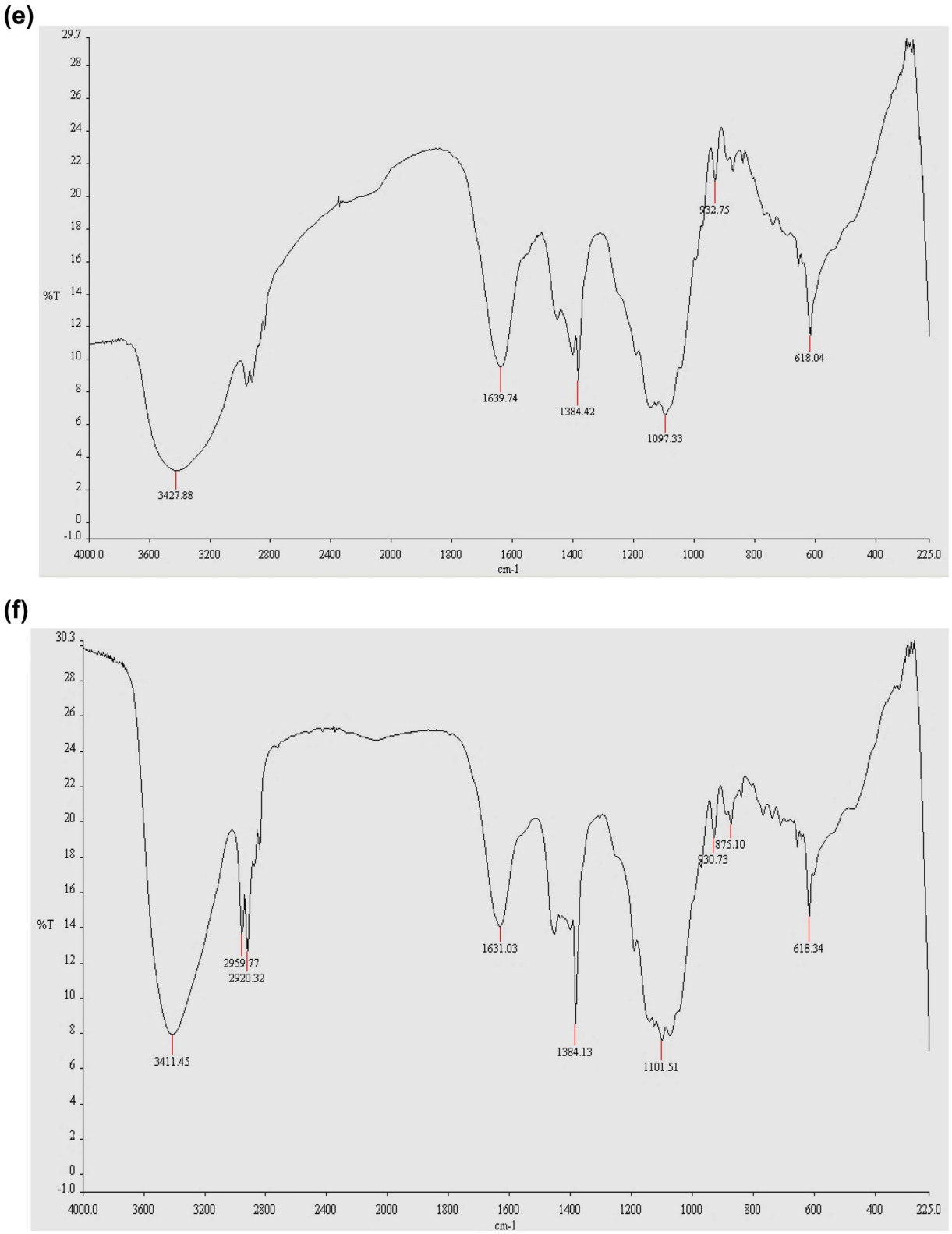

FIGURE 2 (Continued)

musciformis extract, and it was characterised by UV–vis spectra, TEM, EDX, XRD and FTIR. The change of solution colour after the reaction is the primary indication of the formation of Ag/AgCl-NPs. Our synthesised Ag/AgCl-NPs solution colour changed from light red to deep brown after the reaction. The absorbance peak of all reaction solutions was

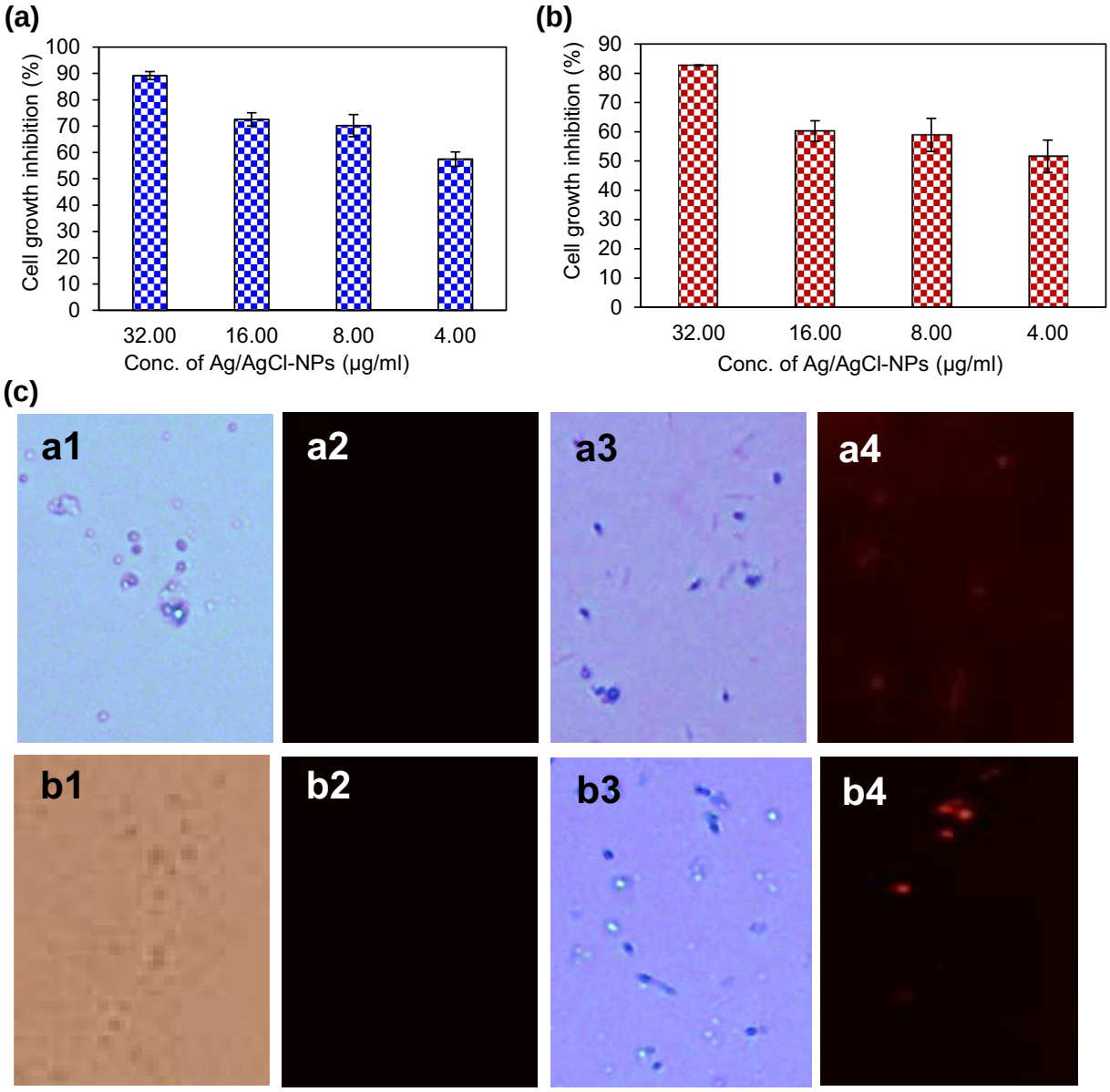

FIGURE 3 Antibacterial activity and detection of possible apoptosis by fluorometric assay. (a) *Staphylococcus aureus* cell growth inhibition in vitro; (b) *Streptococcus mutans* cell growth inhibition in vitro; (c) Ag/AgCl-NPs untreated ('1' and '2') and treated ('3' and '4') bacterial cells were incubated with propidium iodide (PI). 'a' and 'b' indicating *S. mutans* and *S. aureus* bacteria where '1' and '3' representing optical images; '2' and '4' representing fluorometric images after stained with PI

TABLE 1 Zone of bacterial growth inhibition by *Hypnea musciformis* extract-mediated Ag/AgCl-NPs

Zone of bacterial growth inhibition					
	Hypnea musciformis-mediated Ag/AgCl-NPs (µg/ml)				Streptomycin (unit)
Name of bacteria	10	20	40	80	15
Staphylococcus aureus	19.30 ± 1.00	20.50 ± 1.20	21.50 ± 1.00	22.00 ± 1.00	12.00 ± 0.50
Streptococcus mutans	19.00 ± 1.00	20.30 ± 0.75	21.40 ± 1.50	21.70 ± 1.00	11.60 ± 0.25

between 400 and 450 nm determined by UV–visible spectroscopy. A sharp absorbance peak at the wavelength of 425 nm was due to the surface plasmon resonance [30]. The intensity of the solution colour increased with the increase in $AgNO_3$ concentrations for each reaction time that might have happened due to the formation of different sizes of nanoparticles. The highly monodispersed and spherical shape of the majority of particles was observed by TEM. The sizes of the nanoparticles diameter were within the range of 10–80 nm, where an average diameter was 11 nm estimated by image J software. Roni et al. [19] and Vadlapudi and Amanchy [20] reported that *H. musciformis*-mediated Ag/AgCl-NPs

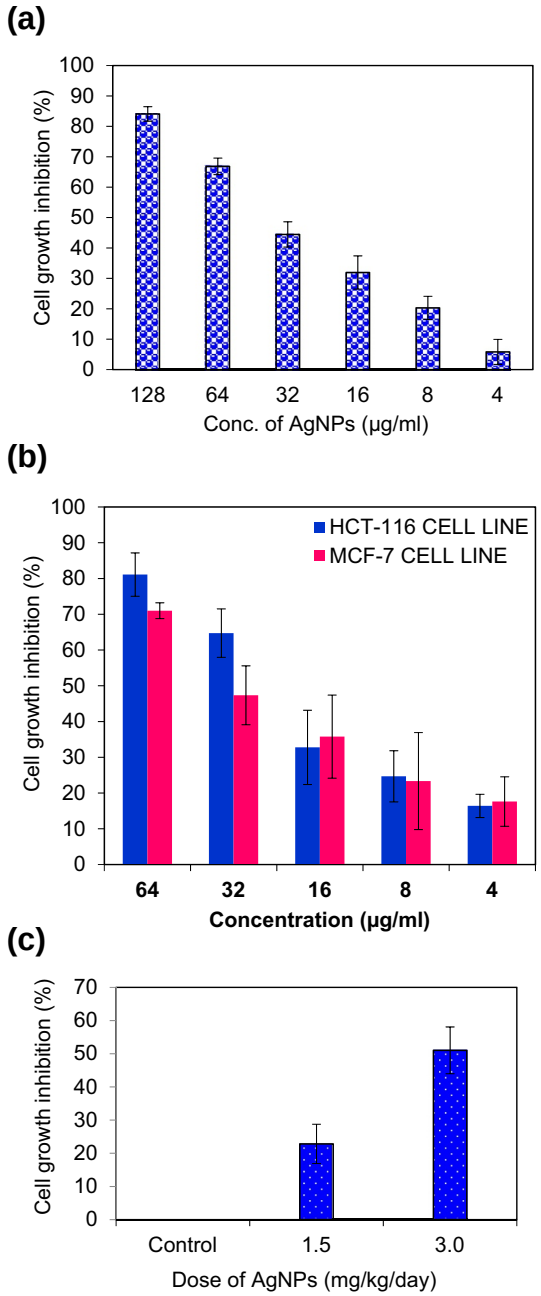

FIGURE 4 Antiproliferative activity of *Hypnea musciformis* extracts mediated Ag/AgCl-NPs. (a) Ehrlich ascites carcinoma (EAC) cell growth inhibition *in vitro;* (b) colorectal cancer (HCT-116) and MCF-7 cell growth inhibition *in vitro;* (c) effect of Ag/AgCl-NPs on EAC cells growth in vivo in mice. Data are expressed in mean ± SD (n = 6)

were spherical, and the size of the diameter was within the range of 40–65 nm and 16–42 nm, respectively. Different cultivated samples, the sample extraction process and reaction conditions might be responsible for forming different sizes of nanoparticles. Several researchers reported that most of the plant-mediated AgNPs were spherical in shape and the average diameters were between 25 and 50 nm [31]. EDX exhibited elemental silver and chlorine ions and signals of carbon and oxygen in Ag/AgCl-NPs. The weak signals can be formed due to the binding of bioactive molecules to the surface of Ag/AgCl-NPs [32]. XRD proved the crystalline nature of the synthesised nanoparticles and showed the peaks for Ag and AgCl. Many scientists reported similar observations [22, 24, 33]. *H. musciformis* extract showed the major peaks at 3427.88, 1639.74, 1384.42, 1097.33 and 618.04 cm^{-1}, whereas 3411.45, 2920.32, 1631.03, 1384.13, 1101.1 and 618.34 cm^{-1} peaks were obtained in synthesised Ag/AgCl-NPs. The peaks at 3427.88 and 3411.45 cm^{-1} indicated the characteristics of the hydroxyl functional group in phenol and alcohol compounds [34]. The peak at 2920.32 cm^{-1} indicated CH stretching of alkanes [30]. The peaks at 1639.74 and 1631.03 indicated the bending vibration of the (NH) C=O group [35]. The peaks at 1384.42 and 1384.13 cm^{-1} indicated stretching for the (N–O) functional group [35].

The peaks at 1097.33 and 1101.1 cm^{-1} indicated a vibration of the (C=O) functional group [30]. The peaks at 618.04 and 618.34 cm^{-1} indicated a vibration of (C–Cl) groups [36]. As compared, we can say that the *H. musciformis* extract and the synthesised Ag/AgCl-NPs share certain common functional groups. Probably, –OH groups might be responsible for reducing Ag+ to Ag° [30]. The band shift in hydroxyl and carbonyl groups in FTIR spectra confirm the oxidation of amines, phenols, alcohols, carboxylic acid and other secondary metabolites of seaweed extract and this shifting is also involved in stabilising/capping the nanoparticles as reported in many studies [37]. Thus, these functional groups may perform a significant role in the reduction of Ag^{+} into Ag/AgCl-NPs. The above-mentioned shift was observed during the nanoparticle formation from various sources of extracts [16, 38].

Inhibition of bacterial growth is a common biological characterisation of AgNPs. In the present study, we have also checked the antibacterial activities of the newly synthesised Ag/AgCl-NPs against pathogenic bacteria by MTT assay, disc diffusion assay and antibiofilm assay. In all cases, synthesised Ag/AgCl-NPs showed good inhibition to both *S. aureus* and *S. mutans*. The synthesised Ag/AgCl-NPs were more effective against both bacteria compared to streptomycin. The exact mechanism of Ag/AgCl-NPs against different bacteria is still unknown. Many scientists reported that AgNPs generate pore/pit in the bacterial cell wall and cause permeability on bacterial cell surfaces, and it increases for small-size nanoparticles. Next, nanoparticles bind the functional groups of DNA and proteins and cellular alteration occurs [39–41]. Bacterial cells were stained with PI to find the molecular mechanism of the antiproliferative activity of Ag/AgCl-NPs. Treated bacterial cells exhibited the induction of apoptosis. Induction of apoptosis in bacterial cells was reported by other scientists as well [41, 42].

Cancer is an uncontrolled proliferation of cells with tremendous lethal effects on patients. For the past few years, the outbreak of cancer has increased worldwide as a most important cause of death. At this point, annually, more than seven million people are being affected by cancer diseases worldwide. However, we have developed cancer diagnosis and treatment, but till now, it is an enormous trouble for society. Seaweeds contain plentiful bioactive compounds, and it has important therapeutic values that have become evident [43]. Some bioactive compounds assist in nanoparticle formation

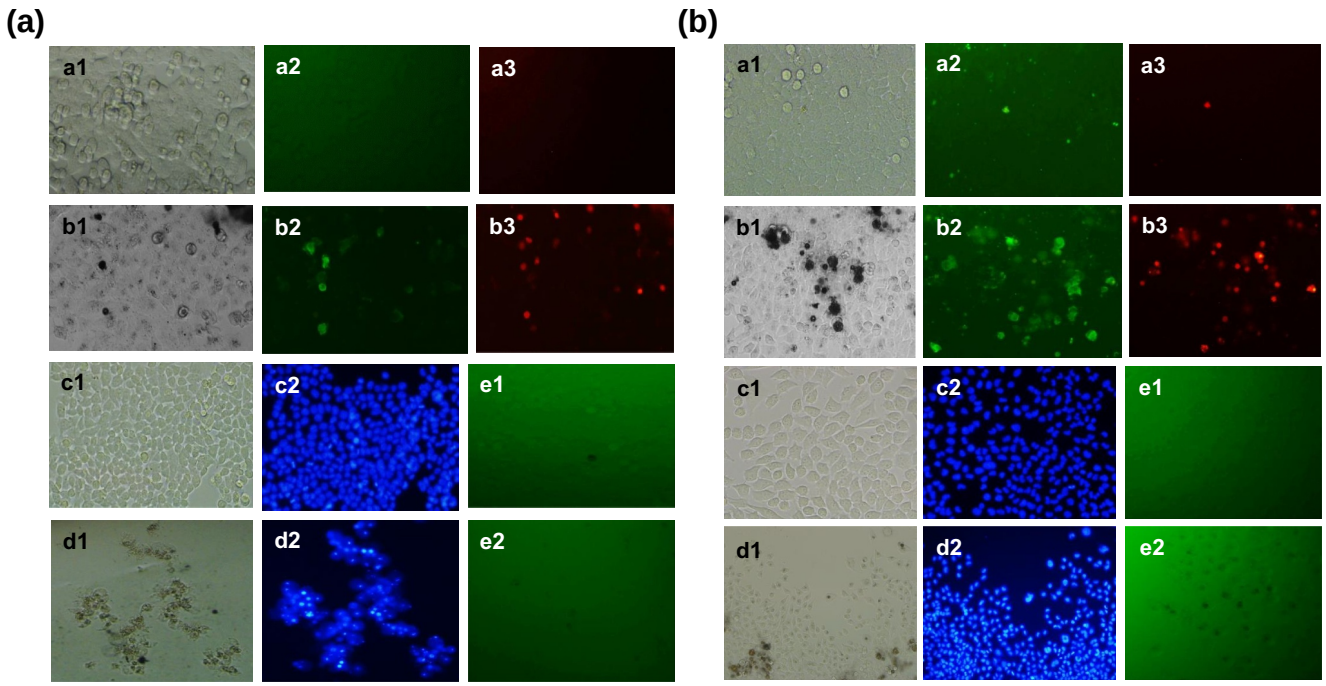

FIGURE 5 Induction of apoptosis and generation of reaction oxygen species by different fluorometric assays (a) and (b) detection of early and late apoptosis in colorectal cancer (HCT-116) and breast cancer (MCF-7) cells, respectively, where '**a**' and '**b**' indicates control and treated cells. '**1**' indicating optical image and '**2**' and '**3**' indicating fluorometric images for early and late apoptosis, respectively. '**c**' and '**d**' indicate control and treated cells stained with Hoechst 33342 dye, where '**1**' indicating optical image and '**2**' indicating fluorometric image. Finally, e1 and e2 indicate fluorometric images for control and treated cells after staining with DCFH-DA. The image was captured at 20× magnification

as reducing and capping agents can be used to develop new drugs against cancer cells. It was reported in the literature that marine plant-mediated nanoparticles have antitumour property [10]. In the present study, we used EAC, HCT-116, and MCF-7 cells to evaluate the antiproliferative activity of *H. musciformis*-mediated Ag/AgCl-NPs and identified strong antiproliferative activity against EAC and MCF-7 cells. The anticancer potential of plant extract-mediated Ag/AgCl-NPs against different cancer cell lines were different. *Zizyphus mauritiana*-assisted Ag/AgCl-NPs showed antiproliferation against EAC cells with the IC_{50} values of 84 μg/ml [22]. *Ulva lactuca* seaweed-assisted AgNPs showed antiproliferation against MCF-7 cells with the IC_{50} values of 37 μg/ml [10]. The IC_{50} values of *oscillatoria*-mediated AgNPs and GM-mediated AgNPs on HCT-116 cells were 5.369 and 40.2 μg/ml, respectively [43, 44].

After cancer cell growth inhibition, we used the dye PI in treated and untreated HCT-116 and MCF-7 cells to know the molecular mechanism of Ag/AgCl-NPs. The induction of apoptosis in treated HCT-116 and MCF-7 cells was exhibited. A similar observation was confirmed when we used the dye FITC-Annexin V. The induction of apoptosis in cells was further verified by using Hoechst 33342 dye. The irregular shape and condense nuclei were visualised in treated cells. Many scientists reported that AgNPs induce apoptosis in a different cancer cell lines [45–49]. Several studies stated that cellular uptake of AgNPs leads to the generation of ROS in cancer cells, which provokes oxidative stress causing apoptosis [22] but we did not find ROS generation in treated HCT-116 and MCF-7 cells. Our study revealed that the synthesised Ag/AgCl-NPs could promote cell death without ROS generation.

In our previous experiments, it was found that after the treatment of MCF-7 cells with the *Zizyphus mauritiana* fruit extract-mediated Ag/AgCl-NPs, the expression of Fas increased that activated the caspase-3 expression, sequentially activating FADD and caspase-8. Finally, PARP was cleaved, and apoptosis was induced in the Fas-mediated pathway [22]. But in this experiment, after the treatment of MCF-7 cells with the *H. musciformis* seaweed extract-mediated Ag/AgCl-NPs, the expression of Fas decreased indicating that the Fas pathway was not involved in this apoptosis process. In another experiment, *Kaempferia rotunda* caused a significant over-expression of NFκB gene in glioblastoma stem cells by activating several genes. Finally, the NFκB entered into the nucleus and broke down DNA, and apoptosis occurred [24]. In the present study, NFκB was not responsible for apoptosis as the expression level of NFκB was not altered. The mitochondrial pathway may not be responsible for this apoptosis process as the expression level of Bcl-2 and BAX decreased. A significant increase in autophagy cell death-related ATG5 gene expression was observed. It indicates that autophagy cell death may also occur in the MCF-7 cells besides apoptosis. After cancer study in vitro using Ag/AgCl-NPs, we used the experiment in vivo on EAC cells. Ag/AgCl-NPs inhibited 22.83% and 51% of the EAC cell growth in vivo in mice when administered 1.5 and 3.0 mg/kg/day (i.p.), respectively, for five consequent days. In our earlier experiments, the

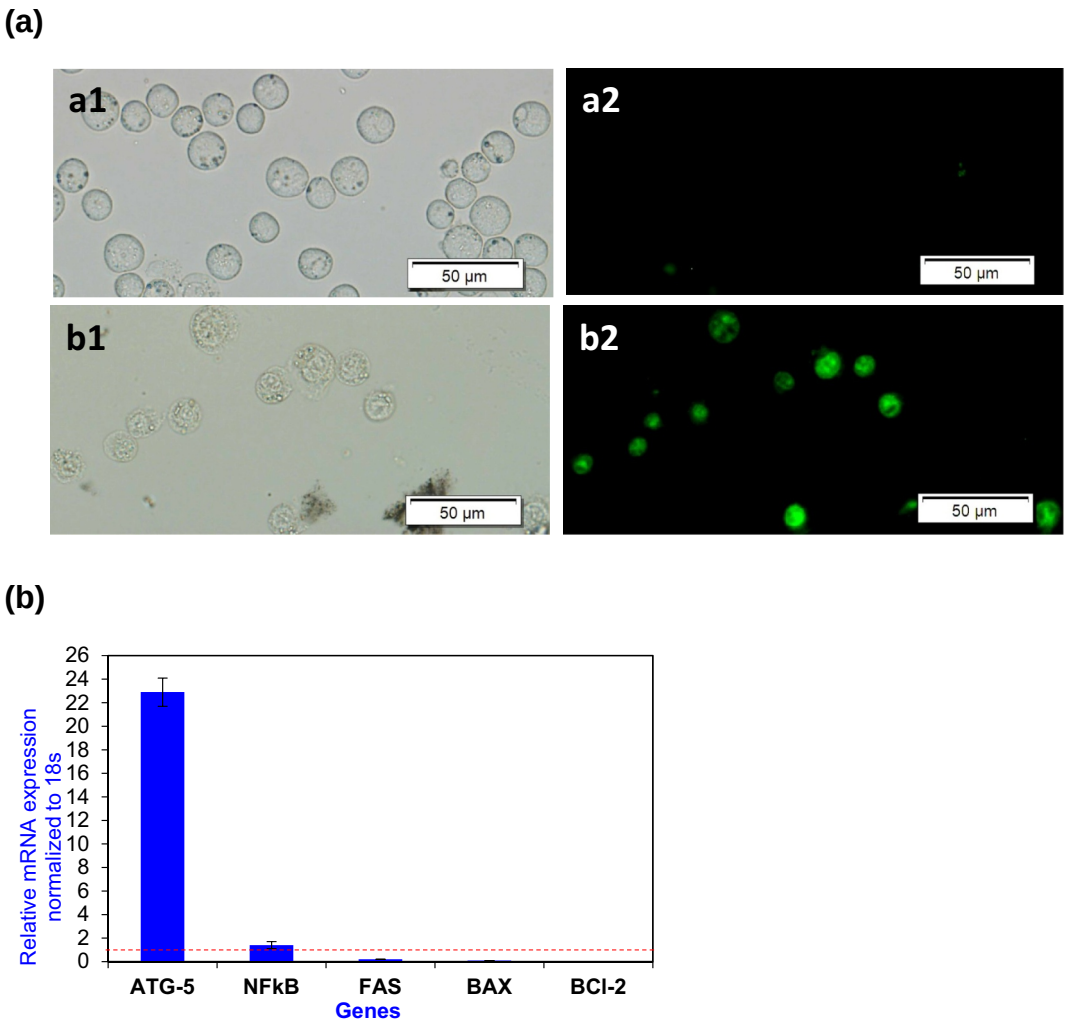

FIGURE 6 Gene and protein expressions. (a) and (b) representing control and treated cells, where '1' and '2' indicate optical and fluorometric views; (b) percentages of relative mRNA expression after treatment of MCF7 cells with Ag/AgCl-NPs

antitumour activity of *K. rotunda* tuberous rhizome and *Z. mauritiana* fruit extract-mediated Ag/AgCl-NPs was checked against EAC cells in vivo in mice. 20% cells growth inhibition was observed for *Z. mauritiana* fruit extract-mediated Ag/AgCl-NPs at the dose of 12 mg/kg/day. On the other hand, at the doses of 6 and 12 mg/kg/day, 32.3% and 55% EAC growth inhibition was monitored. From the results, it is clear that *H. musciformis* seaweed extract-mediated Ag/AgCl-NPs is a more effective anticancer agent than *K. rotunda* and *Z. mauritiana* fruit extract-mediated Ag/AgCl-NPs. Treated and untreated EAC cells were stained with the caspase-3 substrate and a significant level of the caspase-3 protein expression was found in the treated cells that indicated the induction of apoptosis in EAC cells.

5 | CONCLUSIONS

By a cost-effective, simple and eco-friendly approach, Ag/AgCl-NPs were successfully synthesised using *H. musciformis* extract, cultivated in Bangladesh, as a capping and reducing agent. The characteristics of *H. musciformis*-mediated Ag/AgCl-NPs were determined by UV, TEM, EDX, XRD and FTIR. These procedures proved that the synthesised Ag/AgCl-NPs were of spherical shape with an average size of 11 nm and crystalline nature. Remarkable antibacterial activity of synthesised Ag/AgCl-NPs was detected against oral pathogenic bacteria *S. aureus* and *S. mutans*. It has potent anticancer activity against EAC, HCT-116 and MCF-7 cells. Initiation of apoptosis was induced in EAC, HCT-116 and MCF-7 cells using synthesised Ag/AgCl-NPs. Besides, the initiation of apoptosis autophagy cell death occurred in MCF-7 cells.

ACKNOWLEDGEMENTS

These research studies were financed by the Ministry of Science and Technology (Grant No. 39.009.002.01.00.057.2015-2016/922/Phys-362) and the Faculty of Science, the University of Rajshahi, Bangladesh (Grant No. A-930/5/52/RU/Science-30/20-21).

CONFLICT OF INTEREST

The authors of this manuscript have declared no conflict of interest.

DATA AVAILABILITY STATEMENT

Data sharing is not applicable to this article as no datasets were generated or analysed during the current study.

ORCID

Syed Rashel Kabir https://orcid.org/0000-0002-5708-014X

REFERENCES

1. Barton, M.B., Frommer, M., Shafiq, J.: Role of radiotherapy in cancer control in low-income and middle-income countries. Lancet Oncol. 7(7), 584–595 (2006)
2. Uddin, A., et al.: Cancer care scenario in Bangladesh. South Asian J. Cancer. 2, 102–104 (2013)
3. Kithiyon, M., et al.: Efficacy of mycosynthesised AgNPs from *Earliella scabrosa* as an in vitro antibacterial and wound healing agent. IET Nanobiotechnol. 13(3), 339–344 (2019)
4. Kalantari, K., et al.: Autoclave-assisted synthesis of AgNPs in *Z. officinale* extract and assessment of their cytotoxicity, antibacterial and antioxidant activities. IET Nanobiotechnol. 13(3), 262–268 (2019)
5. Ghanbar, F., et al.: Antioxidant, antibacterial and anticancer properties of phyto-synthesised *Artemisia quttensis* Podlech extract mediated AgNPs. IET Nanobiotechnol. 11(4), 485–492 (2017)
6. Goodman, A.M., et al.: The surprising in vivo instability of near-IR-absorbing hollow Au-Ag nanoshells. ACS Nano. 8(4), 3222–3231 (2014)
7. Barabadi, H., et al.: Efficacy of green nanoparticles against cancerous and normal cell lines: a systematic review and meta-analysis. IET Nanobiotechnol. 12(4), 377–391 (2018)
8. Nallathamby, P., Xu, X.-H.N.: Study of cytotoxic and therapeutic effects of stable and purified silver nanoparticles on tumor cells. Nanoscale. 2(6), 942–952 (2010)
9. Sriram, M.I., et al.: Antitumor activity of silver nanoparticles in Dalton's lymphoma ascites tumor model. Int. J. Nanomedicine. 5, 753–762 (2010)
10. Bhimba, V., Bhimba, D.: Anticancer activity of silver nanoparticles synthesized by the seaweed *Ulva lactuca* invitro. J. Nanomed. Biotherap. Discov. 1(4) (2012)
11. Asaduzzaman, A.K.M., Chun, B.-S., Kabir, S.R.: *Vitis vinifera* assisted silver nanoparticles with antibacterial and antiproliferative activity against Ehrlich ascites carcinoma cells. J. Nanopart. 2016, 1–9 (2016)
12. Satapathy, S.R., et al.: Silver-based nanoparticles induce apoptosis in human colon cancer cells mediated through p53. Nanomedicine. 8(8), 1307–1322 (2013)
13. Newman, M.J., et al.: Purification and reconstitution of functional lactose carrier from *Escherichia coli*. J. Biol. Chem. 256(22), 11804–11808 (1981)
14. Paterson, I., Anderson, E.A.: The renaissance of natural products as drug candidates. Science. 310, 451–453 (2005)
15. Černá, M.: Seaweed Proteins and Amino Acids as Nutraceuticals, 1st ed. Elsevier Inc. (2011)
16. Shanmugam, N., et al.: Biosynthesis of silver nanoparticles from the marine seaweed *Sargassum wightii* and their antibacterial activity against some human pathogens. Appl. Nanosci. 4(7), 881–888 (2014)
17. Jayaprakash, P., et al.: Antioxidant and anticancer potential of green synthesized silver nanoparticles of Brown Algae *Sargassum wightii* Greville against Pc-3 human prostate cancer cell line. Eur. J. Pharm. Med. Res. 4(3), 275–287 (2010)
18. Selvam, G.G., Sivakumar, K.: Phycosynthesis of silver nanoparticles and photocatalytic degradation of methyl orange dye using silver (Ag) nanoparticles synthesized from *Hypnea musciformis* (Wulfen) J.V. Lamouroux. Appl. Nanosci. 5(5), 617–622 (2015)
19. Roni, M., et al.: Characterization and biotoxicity of *Hypnea musciformis*-synthesized silver nanoparticles as potential eco-friendly control tool against *Aedes aegypti* and Plutella. Ecotoxicol. Environ. Saf. 121, 31–38 (2015)
20. Vadlapudi, V., Amanchy, R.: Synthesis, characterization and antibacterial activity of silver nanoparticles from red algae. Adv. Biol. Res. 11(5), 242–249 (2017)
21. Venkatesan, J., Kim, S., Shim, M.S.: Antimicrobial, antioxidant, and anticancer activities of biosynthesized silver nanoparticles using marine algae *Ecklonia cava*. Nanomaterials. 6(12), 235 (2016)
22. Kabir, S.R., et al.: *Zizyphus mauritiana* fruit extract-mediated synthesized silver/silver chloride nanoparticles retain antimicrobial activity and induce apoptosis in MCF-7 cells through the Fas pathway. ACS Omega. 5, 20599–20608 (2020)
23. Kabir, S.R., et al.: A new lectin from the tuberous rhizome of *Kaempferia rotunda*: isolation, characterization, antibacterial and antiproliferative activities. Protein Pept. Lett. 18(11), 1140–1149 (2011)
24. Kabir, S.R., et al.: Biogenic silver/silver chloride nanoparticles inhibit human glioblastoma stem cells growth in vitro and Ehrlich ascites carcinoma cell growth in vivo. J. Cell. Mol. Med. 24(September), 13223–13234 (2020)
25. Kabir, S.R., et al.: Pea lectin inhibits growth of Ehrlich ascites carcinoma cells by inducing apoptosis and G2/M cell cycle arrest in vivo in mice. Phytomedicine. 20(14), 1288–1296 (2013)
26. Ahsanul Kabir, K.M., et al.: *Geodorum densiflorum* rhizome lectin inhibits Ehrlich ascites carcinoma cell growth by inducing apoptosis through the regulation of BAX, p53 and NF-κB genes expression. Int. J. Biol. Macromol. 125, 92–98 (2019)
27. Hasan, I., Ozeki, Y., Kabir, S.R.: Purification of a novel chitin-binding lectin with antimicrobial and antibiofilm activities from a Bangladeshi cultivar of potato (*Solanum tuberosum*). Indian J. Biochem. Biophys. 51, 142–148 (2014)
28. Fung, A., Hamid, N., Lu, J.: Fucoxanthin content and antioxidant properties of *Undaria pinnatifida*. Food Chem. 136, 1055–1062 (2013)
29. Asaduzzaman, A.K.M., Imtiaj Hasan, M., Habibur Rahman, A.R.M.T.: Antioxidant and antiproliferative activity of phytoconstituents identified from *Sargassum binderi* seaweed extracts cultivated in Bangladesh. Int. J. Biosci. 16(3), 481–494 (2020)
30. Singh, G., et al.: Green synthesis of silver nanoparticles using cell extracts of *Anabaena doliolum* and screening of its antibacterial and antitumor activity. J. Microbiol. Biotechnol. 10, 1354–1367 (2014)
31. Vanaja, M., et al.: Herbal plant synthesis of antibacterial silver nanoparticles by *Solanum trilobatum* and its characterization. Int. J. Met. 2014, 1–8 (2014)
32. Reddy, M., et al.: Phytosynthesis of eco-friendly silver nanoparticles and biological applications – a novel concept in nanobiotechnology. Afr. J. Biotechnol. 14, 222–247 (2015)
33. Kota, S., et al.: Evaluation of therapeutic potential of the silver/silver chloride nanoparticles synthesized with the aqueous leaf extract of *Rumex acetosa*. Sci. Rep. 7 (2017)
34. Song, J.Y., Jang, H-K., Kim, B.S.: Biological synthesis of gold nanoparticles using *Magnolia kobus* and *Diopyros kaki* leaf extracts. Artic. Process Biochem. 44(10), 1133–1138 (2009)
35. Marimuthu, S., et al.: Evaluation of green synthesized silver nanoparticles against parasites. Parasitol. Res. 108(6), 1541–1549 (2011)
36. Rajeshkumar, S., Kannan, C., Annadurai, G.: Green synthesis of silver nanoparticles using marine brown algae *Turbinaria conoides* and its antibacterial activity. Int. J. Pharm. Biol. Sci. 3(4), 502–510 (2012)
37. Vanaja, M., Annadurai, G.: Coleus aromaticus leaf extract mediated synthesis of silver nanoparticles and its bactericidal activity. Appl. Nanosci. 3(3), 217–223 (2013)
38. Kannan, R.R.R., et al.: Green synthesis of silver nanoparticles using marine macroalga *Chaetomorpha linum*. Appl. Nanosci. 3(3), 229–233 (2013)
39. Sharma, V.K., Yngard, R.A., Lin, Y.: Silver nanoparticles: green synthesis and their antimicrobial activities. Adv. Colloid Interface. 145, 83–96 (2009)
40. Feng, Q.L., et al.: A mechanistic study of the antibacterial effect of silver ions on *Escherichia coli* and *Staphylococcus aureus*. J. Biomed. Mater. Res. 52(4), 662–668 (2000)

41. Hakansson, A.P., et al.: Apoptosis-like death in bacteria induced by HAMLET, a human milk lipid-protein complex. PLoS One. 6(3), e17717 (2011)
42. Dorsey-Oresto, A., et al.: YihE kinase is a central regulator of programmed cell death in bacteria. Cell Rep. 3, 528–537 (2013)
43. Hamouda, R., et al.: Synthesis and biological characterization of silver nanoparticles derived from the cyanobacterium *Oscillatoria limnetica*. Sci. Rep. 9, 13071 (2019)
44. Lee, K.X., et al.: Bio-mediated synthesis and characterisation of silver nanocarrier, and its potent anticancer action. Nanomaterials. 9, 1423 (2019)
45. Baharara, J., et al.: Silver nanoparticles biosynthesized using *Achillea biebersteinii* flower extract: apoptosis induction in MCF-7 cells via caspase activation and regulation of BAX and BCL-2 gene expression. Molecules. 20, 2693–2706 (2015)
46. George, B.P.A., et al.: Apoptotic efficacy of multifaceted biosynthesized silver nanoparticles on human adenocarcinoma cells. Sci. Rep. 8, 1–14 (2018)
47. Barabadi, H., et al.: Emerging theranostic biogenic silver nanomaterials for breast cancer: a systematic review. J. Clust. Sci. 30, 259–279 (2019)
48. Venugopal, K., et al.: Synthesis of silver nanoparticles (Ag NPs) for anticancer activities (MCF 7 breast and A549 lung cell lines) of the crude extract of *Syzygium aromaticum*. J. Photochem. Photobiol. B. 167, 282–289 (2017)
49. Venugopal, K., et al.: The impact of anticancer activity upon *Beta vulgaris* extract mediated biosynthesized silver nanoparticles (Ag-NPs) against human breast (MCF-7), lung (A549) and pharynx (Hep-2) cancer cell lines. J. Photochem. Photobiol. B. 173, 99–107 (2017)

SUPPORTING INFORMATION

Additional supporting information may be found in the online version of the article at the publisher's website.

How to cite this article: Ghose, R., et al.: *Hypnea musciformis*-mediated Ag/AgCl-NPs inhibit pathogenic bacteria, HCT-116 and MCF-7 cells' growth in vitro and Ehrlich ascites carcinoma cells in vivo in mice. IET Nanobiotechnol. 16(2), 49–60 (2022). https://doi.org/10.1049/nbt2.12075